Date of publication xxxx 00, 0000, date of current version xxxx 00, 0000.

Digital Object Identifier 10.1109/TQE.2024.DOI

TAQNet: Traffic-Aware Minimum-Cost Quantum Communication Network Planning

ILORA MAITY[1], (Member, IEEE), JUNAID UR REHMAN[2], SYMEON CHATZINOTAS[1], (Fellow, IEEE)

[1]Interdisciplinary Centre for Security, Reliability and Trust (SnT), University of Luxembourg, Luxembourg (email: {ilora.maity, symeon.chatzinotas}@uni.lu)
[2]Department of Electrical Engineering, and the Center for Intelligent Secure Systems, King Fahd University of Petroleum and Minerals (KFUPM), Dhahran 31261, Saudi Arabia (email: junaid.urrehman@kfupm.edu.sa)

Corresponding author: Ilora Maity (email: ilora.maity@uni.lu).

This work was supported by the project Lux4QCI (GA 101091508) funded by the Digital Europe Program and the project LUQCIA funded by the Government of Luxembourg/SMC.
A preliminary version of this work is published in IEEE Globecom Workshops 2023, Kuala Lumpur, Malaysia (December 04-08, 2023), DOI: 10.1109/GCWkshps58843.2023.10464831.

ABSTRACT Quantum key distribution (QKD) provides a secure method to exchange encrypted information between two parties in a quantum communication infrastructure (QCI). The primary challenge in deploying a QCI is the cost of using optical fibers and trusted repeater nodes (TRNs). Practical systems combine quantum and classical channels on the same fiber to reduce the cost of fibers dedicated to QKD. In such a system with quantum-classical co-existence, the optimal distribution of QKD requests with minimal deployment cost and power usage on the multiplexed links is challenging due to the diverse key rate demands of the requests, number of classical and quantum channels, guard band spacing between classical and quantum channels, and secret key rate of the quantum channels that decreases with distance. To address these challenges, in this work, we propose a Steiner tree-based approach for constructing a QCI that connects all quantum nodes with minimum TRNs. In addition, we propose a genetic algorithm-based solution to optimally distribute the end-to-end (E2E) QKD requests over the QCI. We also determine feasible optical bypass routes to reduce the overall energy consumption in the network further. The proposed approach reduces the QCI deployment cost by 19.42% compared to the benchmark MST-Baseline. Also, on average, TAQNet with optical bypass achieves 4.69 kbit per Joule more energy efficiency compared to the non-bypass approach.

INDEX TERMS Quantum Communication Infrastructure (QCI), Quantum Key Distribution (QKD), Network Planning, Steiner Tree, Genetic Algorithm (GA), Optical Bypass.

I. INTRODUCTION

In the evolving landscape of information exchange, quantum communication promises a revolutionary shift in data transmission, security, and processing [1]. A quantum communication infrastructure (QCI) deployed over a classical network infrastructure [2] extends the capabilities of the classical network substantially in terms of data security, which is a necessity of modern-age network applications such as e-banking or e-health applications [3]. QCI enables quantum key distribution (QKD) [4] that promises secure information exchange between a pair of quantum nodes (QNs) by distributing symmetric secret keys [5]. The secret keys encrypt sensitive messages for transmission over public channels [6] [7]. Also, the no-cloning theorem prevents passive eavesdropping on the transmitted message [8].

A. MOTIVATION

QCI consists of QNs to generate, exchange, and measure quantum states and trusted repeater nodes (TRNs) to distribute secret keys to distant QNs [9]. Given the extensively deployed fiber optics network, it is convenient to build QCI over a classical network to reduce the infrastructure cost of having a dedicated QCI [3]. In a quantum communication network integrated with a classical network, quantum and

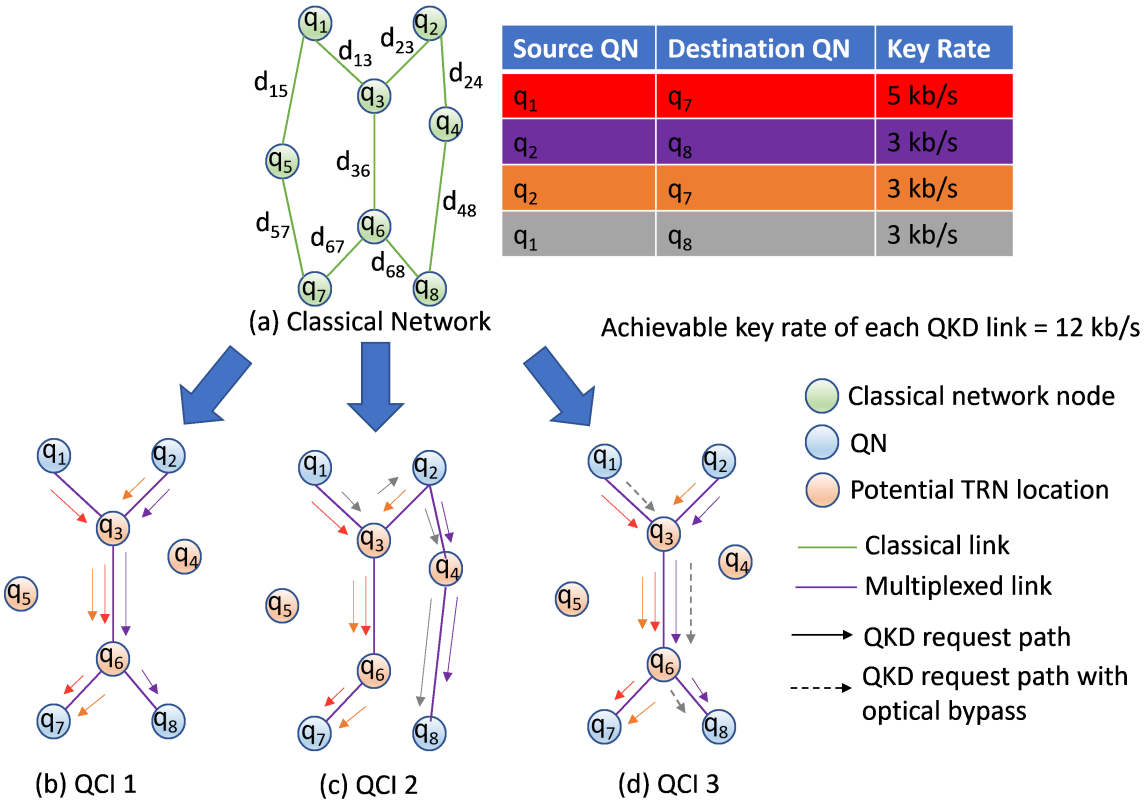

FIGURE 1: Example of classical-quantum co-existence with different minimum QCI deployments

classical channels can coexist on the same optical fiber by using wavelength division multiplexing (WDM) [4]. In such a WDM network, classical channels transmit data and classical bits for QKD authentication and critical classical post-processing steps of QKD (e.g., information reconciliation, parameter estimation, privacy amplification). However, we expect the traffic of this auxiliary channel to be marginal compared to the volume of digital communication. The quantum channel transmits quantum signals [10].

In this paper, we adopt the BB84 protocol [11] for QKD, one of the most widely studied and implemented protocols, due to its robustness and simplicity in practical settings. BB84 is well-suited for our scenario because it provides a strong foundation for key generation using a trusted relay approach and complements the classical infrastructure. While other QKD protocols, such as E91 [12] and measurement-device-independent (MDI) QKD [13], offer advantages like entanglement-based security and enhanced robustness against specific types of attacks, they introduce increased complexity. This complexity results in a more intricate system model for routing and necessitates distinct architectural considerations. Therefore, for simplicity, we consider BB84 a more appropriate choice for initial deployment in a mixed classical-quantum network environment. QKD is realized with a QKD transmitter and a receiver placed at the QNs linked via the multiplexed optical fiber serving as the QKD link. For QKD between non-adjacent QNs, secure keys traverse intermediate QNs and TRNs through the multiplexed optical fiber links, maintaining the required key rate [8]. Another option is to use the technique of optical bypass to connect non-adjacent QNs bypassing the IP layer of the intermediate nodes [14]. Optical bypass reduces overall power consumption of the network by eliminating the power consumed at the router ports of the intermediate nodes. However, the link attenuation increases with distance, diminishing the key rate for long bypass paths.

A cost-effective QCI deployment reduces the fiber usage by connecting all QNs with the minimum number of TRNs in a spanning tree [15]. However, in practice, QKD requests have specific key rate requirements. Also, the secret key rate (SKR) on each link is limited based on the distance as the quantum signal attenuates with distance. This also limits the setting of long optical bypass links. For example, Figure 1 shows two spanning trees for minimum QCI deployment in Figure 1(b) and 1(c) over the classical network in 1(a). In this example, we consider 4 QKD requests (q_1, q_7), (q_2, q_8), (q_2, q_7), and (q_1, q_8), with key rates 5 kb/s, 3 kb/s, 3 kb/s, and 3 kb/s, respectively. Although considered fixed to 12 kb/s in this example, the SKR of QKD links varies as the key rate decreases with distance and fiber attenuation. Based on the QCI deployment of 1(b), we can assign the requests (q_1, q_7), (q_2, q_8), and (q_2, q_7) to the paths $q_1 \rightarrow q_3 \rightarrow q_6 \rightarrow q_7$,

$q_2 \rightarrow q_3 \rightarrow q_6 \rightarrow q_8$, and $q_2 \rightarrow q_3 \rightarrow q_6 \rightarrow q_7$, respectively. However, the request (q_1, q_8) cannot be assigned to the path $q_1 \rightarrow q_3 \rightarrow q_6 \rightarrow q_8$ because the key rate of the link $q_3 \rightarrow q_6$ is not sufficient to accommodate this request. On the other hand, the QCI deployment of 1(c) can accommodate all 4 requests by assigning the requests (q_2, q_8) and (q_1, q_8) to paths $q_2 \rightarrow q_4 \rightarrow q_8$ and $q_1 \rightarrow q_3 \rightarrow q_2 \rightarrow q_4 \rightarrow q_8$. In addition, Figure 1(d) shows that the QKD request (q_1, q_8) can be served using the optical bypass link. Although both classical and quantum traffic can be bypassed, for simplicity, this example focuses on bypassing QKD requests only. In this case, the bypassed QKD request (q_1, q_8) utilizes the path $q_1 \rightarrow q_3 \rightarrow q_6 \rightarrow q_8$ but avoids the IP layer at intermediate nodes q_3 and q_6. The end nodes, q_1 and q_8, are aware of this optical bypass, and all intermediate nodes in the path are assumed to be trusted by both parties to maintain the security of the QKD exchange. The bypass route avoids conventional routing functions at intermediate nodes, ensuring a more direct and secure transmission for quantum traffic. Therefore, deploying QKD involves addressing both end-to-end (E2E) requirements, such as traffic and key rates, and network constraints, including classical-quantum multiplexing in a single fiber using WDM, power consumption, and attenuation considerations.

B. CONTRIBUTION

In this work, we propose a network planning approach for QCI, named TAQNet, that jointly optimizes the capital expenditure (CAPEX) due to the deployment and connectivity of QNs and TRNs, and the operational expenditure (OPEX) in terms of power usage due to co-existing classical and QKD demands. TAQNet constructs a minimal Steiner tree that includes all QNs and places TRNs at selected locations to reduce the CAPEX. In addition, a genetic algorithm (GA)-based solution is designed to optimally orchestrate the QKD demands considering the SKR of the multiplexed links. Moreover, a greedy heuristic algorithm is proposed to identify potential E2E bypass routes for classical and QKD demands for additional reduction of the network energy consumption. The main contributions of the work are as follows:

- We formulate the demand-aware minimum cost QCI deployment problem as a binary integer linear programming (BILP) problem to jointly reduce infrastructure cost and energy consumption due to classical-quantum multiplexing. The BILP considers QKD demands with link attenuation and SKR.
- Finding the global optimal solution of the formulated BILP involves searching the solution space of all possible QCI topologies, QKD orchestrations, and bypass possibilities, which leads to exponential computational complexity. Therefore, we decompose the BILP into three sub-problems (SPs) –(SP1) minimum QCI deployment, (SP2) QKD request orchestration, and (SP3) bypass route selection. We propose a Steiner-tree-based heuristic algorithm to solve SP1 and determine the minimum-cost QCI connecting all QNs. For SP2, we also design a GA-based meta-heuristic algorithm. SP1 and SP2 are solved iteratively until convergence. Finally, we design a greedy heuristic algorithm to evaluate potential bypass routes for classical and QKD demands in the QCI.
- We perform extensive simulations to analyze the performance of TAQNet for varying network conditions, such as the number of quantum channels, QKD traffic, and network topology. We also compare the proposed sub-optimal solution with the optimal solution.

The simulation results show the TAQNet's effectiveness in minimizing the network energy consumption and the number of TRNs in the QCI. Additionally, the performance evaluation explores the trade-offs between QCI cost savings and different network topologies and scales, showing how the benefits of TRN placement and minimum QCI vary with topology. These insights provide a deeper understanding of how TAQNet adapts to diverse network conditions.

C. PAPER ORGANIZATION

The remaining sections of the paper are organized as follows. Section II discusses the work related to minimum QCI deployment, QKD with classical-quantum co-existence, and QKD request orchestration. Section III describes the system model. Section IV formulates the joint optimization problem. Section V decomposes the problem into sub-problems and states the proposed solution approach. Section VI discusses the simulation results. Finally, Section VII concludes the paper and states future work.

II. RELATED WORK

This section presents recent works on minimum QCI deployment, QKD with classical-quantum co-existence, and QKD request orchestration.

A. MINIMUM QCI DEPLOYMENT

Heuristic algorithms for minimum spanning tree (MST) and single-source shortest path tree were proposed by Gunkel et al. [16] to connect all QNs with the shortest possible fiber length. However, the study did not examine the scalability of heuristic solutions concerning QCI size. A span aggregation algorithm that minimizes the number of TRNs in the network was proposed by Patri et al. [6]. This method uses the QNs' transmission limit to determine TRN locations dynamically.

B. QKD WITH CLASSICAL-QUANTUM CO-EXISTENCE

Some works investigate classical-quantum co-existence for QKD. In such networks, the noise generated from the classical signals interferes with the quantum signals, reducing the key rate, particularly over long distances. Kong et al. [3] proposed simultaneous transmission architecture for long-distance QKD and classical signals. The authors compute SKRs considering the influence of noises from classical signals. Another work in [4] demonstrates QKD using the

TABLE 1: Table of symbols

Symbol	***Definition***	***Symbol***	***Definition***
G	Integrated classical-quantum network	G^T	Minimum-cost QCI
$\mathcal{V}$	Set of nodes	$\mathcal{V}^T$	Set of nodes in the minimum-cost QCI
$\mathcal{E}$	Set of multiplexed links	$\mathcal{E}^T$	Set of links in the minimum-cost QCI
$\mathcal{V}^Q$	Set of QNs	P_{dark}	Dark count probability
$\mathcal{V}^R$	Set of TRNs	P_{srs}	SRS noise
δ	Channel spacing	β	Alignment of optical system
B^{guard}	Guard band	μ	Average photon flux
d_{ij}	Distance of $e_{ij} \in \mathcal{E}$	η_i	Transmittance of q_i's equipment
w_{ij}	Attenuation of $e_{ij} \in \mathcal{E}$	η_{spd}	Efficiency of single-photon detector
D_{ij}^C	Classical traffic between q_i and q_j	D_{ij}^Q	QKD traffic between q_i and q_j
$\mathcal{F}^Q$	Set of QKD requests	q_k^{src}	Source QN of $f_k \in \mathcal{F}$
q_k^{dest}	Destination QN of $f_k \in \mathcal{F}$	r_k	Secret key rate demand of $f_k \in \mathcal{F}$
c^Q	QN deployment cost	c^R	TRN deployment cost
c^L	Cost per kilometer of a channel on a fiber link	E^r	Power consumption of a router port
E^t	Power consumption of each transponder	E^e	Power consumption of each EDFA
E^{tr}	Power consumption of each QKD transceiver	B^C	Capacity of classical channel
B^Q	Capacity of quantum channel	N	Number of channels
N^C	Number of classical channels	N^Q	Number of quantum channels
N_{ij}^u	Number of used classical channels between q_i, q_j	N_{ij}^{qu}	Number of used quantum channels between q_i, q_j
A_{ij}	Number of EDFA between q_i and q_j	S	Span distance between two neighboring EDFAs
$D_{ij}^{C,\text{byp}}$	Classical demand on bypass route between q_i, q_j	$D_{ij}^{Q,\text{byp}}$	QKD demand on bypass route between q_i, q_j

temporal-filtering effect to address the trade-off between QKD distance and SKR. The experiment setup allows QKD at a high rate over fibers up to 90 km in length. In recent work, Geng et al. [17] implemented QKD over a WDM network where quantum and classical signals co-exist. The proposed QKD system achieves an SKR of 11 kbps over an optical fiber of 20 km length. The authors in [18] have shown experimentally that a channel spacing of 200 GHz can reduce the interference of the classical signal on the quantum signal significantly. Lin et al. [10] proposed a channel allocation strategy with minimum spontaneous Raman scattering (SRS) to accommodate classical and quantum signals in a dense WDM system.

C. QKD REQUEST ORCHESTRATION

To satisfy the key rate demand of QKD requests, Cao et al. [9] proposed a heuristic algorithm to minimize the cost of deploying QKD over a WDM network. However, only limited-range networks can benefit from this work. Zhang et al. [8] maximizes the number of served QKD requests considering key storage and optical bypass.

Existing literature does not consider serving QKD requests with a reduced QCI cost considering essential factors such as energy consumption due to quantum-classical multiplexing and diverse QKD demands. Therefore, in this work, we iteratively optimize both the deployment cost of QCI and the QKD demands over an integrated classical-quantum network. Also, different from existing works, this work considers the effects of both classical and QKD demands on the QCI cost. Accordingly, we propose bypass routes for both classical and QKD demands to reduce energy consumption.

III. SYSTEM MODEL

As shown in Figure 1, we consider an integrated network $G = (\mathcal{V}, \mathcal{E})$ where quantum and classical signals co-exist over a single optical fiber using WDM. The set of nodes is represented by $\mathcal{V}$, and $\mathcal{E}$ denotes the set of bidirectional links. Each node is capable of transmitting classical signals. In addition, some of these nodes are QNs that can generate, transmit, receive, and measure quantum states to establish secure encrypted keys between two QNs [19], and the other nodes are potential locations for deploying TRNs that can distribute the keys to the distant QNs [20]. Therefore, TRNs enable long-distance QKD, effectively overcoming the limitation of quantum signals that cannot be amplified. TRNs can use encryption techniques such as one-time pad (OTP) to transfer keys between QNs securely [9]. Given that the QKD key rate may be significantly lower than the traffic bitrate, additional encryption techniques such as AES can be implemented, adjusting the key refresh rate accordingly. Let $\mathcal{V}^Q \subset \mathcal{V}$ and $\mathcal{V}^R \subset \mathcal{V}$ denote the sets of QNs and potential TRN locations co-exist with classical network nodes, respectively. On the other hand, $\mathcal{E}$ represents the set of links multiplexing classical and quantum signals. In this work, we consider a dense WDM (DWDM) system where both classical and quantum signals use C-band (1530 - 1565 nm) to facilitate a high SKR and long transmission distance [10] [21]. Following the wavelength allocation strategy in

IEEE Transactions on Quantum Engineering

[21], we consider N channels with $\delta = 100$ GHz channel spacing for the quantum and classical channels. Additionally, we assume $B^{\text{guard}} = 200$ GHz (2 channels) guard band between classical and quantum channels to reduce the effect of noise generated by classical signals on quantum signals. The distance and attenuation of a link $e_{ij} \in \mathcal{E}$ are denoted by d_{ij} and w_{ij}, respectively. Table 1 shows the primary symbols used in this paper.

The CAPEX of a QCI deployment includes the cost of deploying QNs and TRNs and links connecting the nodes. The minimum-cost QCI deployment is represented by $G^T = (\mathcal{V}^T, \mathcal{E}^T)$ with $\mathcal{V}^T \subset \mathcal{V}$ and $\mathcal{E}^T \subset \mathcal{E}$. G^T spans all QNs and a subset of locations for TRN placement. The following binary variable expresses the inclusion of a link from G to G^T:

$$x_{ij} = \begin{cases} 1 & \text{if } e_{ij} \in \mathcal{E} \text{ is in } \mathcal{E}^T, \\ 0 & \text{otherwise.} \end{cases} \tag{1}$$

A. QKD MODEL

This paper considers the standard BB84 protocol [11] for QKD. Two QNs exchange secure keys through a direct link or a fully trusted relay with intermediate TRNs [22]. Two primary metrics used to measure the performance of QKD are the SKR and quantum bit error rate (QBER). The QBER for secure key exchange between $q_i \in \mathcal{V}$ and $q_j \in \mathcal{V}$ is:

$$\text{QBER}_{ij} = \frac{1}{g_{ij}}[\frac{1}{2}Y_0 + \beta[1 - e^{-\mu\eta_{ij}}]], \tag{2}$$

where $Y_0 = 2P_{\text{dark}} + P_{\text{srs}}$ is the system noise that includes the dark count probability P_{dark} and SRS noise P_{srs} split between two QKD devices with phase shift keying-based classical communication [23]. Furthermore, β is the alignment of the optical system, μ is the average photon flux [10], η_{ij} is the channel transmittance [23], and $g_{ij} = Y_0 + 1 - e^{-\mu\eta_{ij}}$ is the gain of the signal state [24] with Y_0 being the yield. The channel transmittance between q_i and q_j is estimated as:

$$\eta_{ij} = 10^{-\frac{w_{ij}d_{ij}}{10}}\eta_i\eta_{\text{spd}}, \tag{3}$$

where η_i is the transmittance of q_i's equipment and η_{spd} is the efficiency of a single-photon detector. For single-photon state, the gain is $g^1_{ij} = Y_1\mu e^{-\mu}$ [25] with $Y_1 \approx Y_0 + \eta$.

The SKR between $q_i \in \mathcal{V}$ and $q_j \in \mathcal{V}$ for practical decoy state protocols is expressed as:

$$r_{ij} \geq g^1_{ij}\left[1 - H\left(\frac{Y_0 + \beta\eta_{ij}}{Y_1}\right)\right] - g_{ij}H(\text{QBER}_{ij})f(\text{QBER}_{ij}), \tag{4}$$

where $H(\cdot)$ is the Shannon binary entropy function, and $f(\cdot)$ is the error correction inefficiency factor function [10] [23].

B. SRS NOISE MODEL

SRS is a nonlinear optical effect where the power from higher-wavelength (Stokes) signals is transferred to lower-wavelength (anti-Stokes) signals, leading to noise in the system. This effect becomes particularly significant when multiple classical and quantum channels coexist on the same fiber, making SRS the primary noise source in such systems [23], [10]. The SRS noise impacts the system's performance by introducing in-band noise that interferes with the quantum signals, and it directly influences the wavelength allocation strategy on a multiplexed link to minimize this interference. The SRS noise on link e_{ij} for N^C classical and N^Q quantum channels for co- and counter-propagating cases are given by:

$$P^{\text{co}}_{\text{srs}} = d_{ij}\exp(-w_{ij}d_{ij})\eta_{spd}\frac{\tau}{h\nu}\sum_{k=1}^{N^Q} E_0\Upsilon(n_{q,k}), \tag{5}$$

$$P^{\text{counter}}_{\text{srs}} = \frac{1}{2w_{ij}}[1-\exp(-2w_{ij}d_{ij})]\eta_{\text{spd}}\frac{\tau}{h\nu}\sum_{k=1}^{N^Q} E_0\Upsilon(n_{q,k}), \tag{6}$$

where τ is the detection gate length, $h\nu$ is the photon energy from the classical channels with average frequency ν where h is the Planck's constant (6.626×10^{-34} Joule seconds), E_0 is the launch power of a classical channel, $n_{q,k}$ refers to the k^{th} quantum channel, and $\Upsilon(n_{q,k})$ denotes the effective SRS co-efficient.

The effective SRS co-efficient can be expressed as [10]:

$$\begin{aligned}
&\sum_{k=1}^{N^Q}\Upsilon(n_{q,k}) \\
&= \sum_{k=1}^{N^Q}\Bigg[\sum_{n_c=1}^{n_{q,k}-1} s_1[n_{q,k} - n_c] + \sum_{n_c=n_{q,k}+1}^{N} s_2[n_c - n_{q,k}] \\
&\quad - s_1\sum_{l=1}^{k-1}[n_{q,k} - n_{q,l}] - s_2\sum_{l=k+1}^{N^Q}[n_{q,l} - n_{q,k}]\Bigg],
\end{aligned} \tag{7}$$

where N is the total number of channels, n_c denotes a classical channel, s_1 and s_2 are the slopes of the frequency dependence of the Stokes and anti-Stokes SRS coefficient.

C. TRAFFIC MODEL

This work considers two types of demands – classical and QKD. Let D^C_{ij} be the classical demand in Gbps between a pair of nodes $q_i \in \mathcal{V}$ and $q_j \in \mathcal{V}$. For the QKD traffic, there exist two cases – (1) all traffic is QKD encrypted, and (2) only sensitive traffic is QKD encrypted. In the first case, the QKD demand D^Q_{ij} is proportional to D^C_{ij}, i.e., $D^Q_{ij} = \zeta D^C_{ij}$, where $\zeta \in (0, 1)$ is the proportionality constant. For the second case, D^Q_{ij} is independent.

The QKD request set is $\mathcal{F}^Q$ during each time period. In this work, we primarily consider a quasi-static set of QKD requests. In core networks where a large number of flows are multiplexed, the requests do not fluctuate aggressively over time. This makes the quasi-static approach applicable, as demands remain stable over certain periods. For example, in large-scale multiplexing environments like backhauling, the slow evolution of requests allows us to define these time periods based on the stability of the demand patterns. Each request $f_k \in \mathcal{F}^Q$ is represented by a tuple $\{q^{\text{src}}_k, q^{\text{dest}}_k, r_k\}$, where $q^{\text{src}}_k \in \mathcal{V}^Q$ is the source QN, $q^{\text{dest}}_k \in \mathcal{V}^Q$ is the destination QN, r_k is the secret key rate demand. In this work, we assume that the requests are constantly active, e.g., backhauling between local distribution networks. Therefore, we consider $\sum_{f_k \in \mathcal{F}^Q} r_k = D^Q_{ij}$ given $q^{\text{src}}_k = q_i \in \mathcal{V}^Q, q^{\text{dest}}_k = q_j \in \mathcal{V}^Q, \forall f_k \in \mathcal{F}^Q$ if all traffic is QKD encrypted. For simplicity, we assume that the key stream duration is the same for

all requests generated simultaneously. Each QKD request f_k is relayed through a set of QKD links to reach from the source QN to the destination QN. It is worth mentioning that the control signaling over the classical systems to establish the E2E keys from P2P ones is marginal and can be ignored. The following binary variable denotes if a request f_k is relayed through a QKD link:

$$y_{ij}^k = \begin{cases} 1 & \text{if } f_k \text{ is relayed through } e_{ij} \in \mathcal{E}, \\ 0 & \text{otherwise.} \end{cases} \quad (8)$$

D. QCI COST MODEL

1) Capital Expenditure (CAPEX)

The CAPEX includes the cost of deploying nodes (QNs and TRNs) and establishing quantum links between the deployed nodes. In real-world scenarios, CAPEX is heavily influenced by factors such as installing advanced physical security systems for TRNs, costs associated with environmental controls in sensitive quantum environments, and implementing redundancy measures to ensure network reliability.

a: Node Deployment Cost

The cost of deploying a QN and a TRN is denoted by c^Q and c^R, respectively. This deployment cost includes the cost of deploying transceivers, multiplexers/demultiplexers, and setting up the security infrastructure (both physical and digital). Therefore, the cost for deploying nodes in $\mathcal{G}^T$ is:

$$\mathcal{C}^N = \sum_{q_i \in \mathcal{V}^Q, \exists e_{ij} \in \mathcal{E}^T} x_{ij} c^Q + \sum_{q_i \in \mathcal{V}^R, \exists e_{ij} \in \mathcal{E}^T} x_{ij} c^R. \quad (9)$$

b: Quantum Link Deployment Cost

The cost of a quantum link depends on two cases – (1) the optical fiber is not available, implying deployment of new fibers, and (2) the optical fiber exists but is inefficiently used in terms of multiplexing because of the quantum-classical separation guard band. For the first case, the deployment cost of e_{ij} is $c_{ij} = c^L N d_{ij}$, where c^L denotes the deployment cost per kilometer of a channel on a fiber link and N is the total number of channels on the link. For the second case, the deployment cost is $c_{ij} = c_{ij}^{L,\text{ext}}$. Therefore, the total deployment cost for QKD links in the QCI is:

$$\mathcal{C}^L = \sum_{e_{ij} \in \mathcal{E}} x_{ij} c_{ij}. \quad (10)$$

Therefore, the CAPEX is given by:

$$\mathcal{C}^{\text{CAP}} = \mathcal{C}^N + \mathcal{C}^L. \quad (11)$$

2) Operating Expenditure (OPEX)

The operating expenditure (OPEX) refers to the network power consumption, which depends on the power consumed by classical and quantum components.

a: Power Consumption of Classical Components

Based on the work in [14], the power consumed by classical components is given by:

$$E^C = \sum_{q_i \in \mathcal{V}} E^r [\Delta_i^C + \sum_{q_j \in \mathcal{V}, i \neq j} N^C] + \sum_{q_i \in \mathcal{V}} \sum_{q_j \in \mathcal{V}_i} E^t N_{ij}^u + \sum_{q_i \in \mathcal{V}} \sum_{q_j \in \mathcal{V}_i} E^e A_{ij}, \quad (12)$$

where E^r, E^t, and E^e are the power consumption of a router port, each transponder, and each Erbium Doped Fiber Amplifiers (EDFA). The number of ports used to collect the data traffic from peripheral access routers to node q_i is $\Delta_i^C = \left\lceil \frac{\sum_{q_j \in \mathcal{V}} D_{ij}^{C,*}}{B} \right\rceil$, where $D_{ij}^{C,*}$ is the classical traffic traversing e_{ij} and B is the transmission capacity of each channel in Gbps [26]. The number of classical channels in each multiplexed QKD link is N^C. Let $N_{ij}^u \leq N^C$ denotes the number of used classical channels between q_i and q_j. The number of EDFA on the link between q_i and q_j is denoted as $A_{ij} = \lceil \frac{d_{ij}}{S} - 1 \rceil + 2$, where S is span distance between two neighboring EDFAs [27].

b: Power Consumption of Quantum Components

The power consumed by the quantum component is:

$$E^Q = \sum_{q_i \in \mathcal{V}} E^r [\Delta_i^Q + \sum_{q_j \in \mathcal{V}, i \neq j} N^Q] + \sum_{q_i \in \mathcal{V}} \sum_{q_j \in \mathcal{V}_i} E^{tr} N_{ij}^{qu}, \quad (13)$$

where $\Delta_i^Q = \left\lceil \frac{\sum_{f_k \in \mathcal{F}^Q} y_{ij}^k r_k}{B} \right\rceil$, $N^Q = N - N^C$ is the number of quantum channels in each multiplexed QKD link, and $N_{ij}^{qu} \leq N^Q$ denotes the number of used quantum channels between q_i and q_j. The power consumption of a QKD transceiver is denoted by E^{tr}.

The OPEX or total power consumption is given by:

$$\mathcal{C}^{\text{OP}} = E^C + E^Q. \quad (14)$$

Both classical and quantum traffic can utilize the optical bypass technique to save energy as the IP router ports on the intermediate nodes are bypassed [14]. The OPEX with or without bypass route can be estimated using (14). For example, let $D_{ij}^{C,\text{byp}}$ and $D_{ij}^{Q,\text{byp}}$ denote the classical and quantum demands shifted from e_{ij} to a bypass route. Let $\mathcal{F}^b \subset \mathcal{F}^Q$ denote the set of bypassed QKD requests. In this case, the OPEX reduces by $E^r \left[\lceil \frac{D_{ij}^{C,byp}}{B} \rceil + \lceil \frac{D_{ij}^{Q,byp}}{B} \rceil + N \right]$ for bypassing a link e_{ij}. Bypassing multiple intermediate links to connect two end nodes is also possible.

We define the following binary variable to denote if a bypass route exists between two nodes:

$$z_{ij} = \begin{cases} 1 & \text{if a bypass route exists between } q_i \text{ and } q_j, \\ 0 & \text{otherwise.} \end{cases} \quad (15)$$

Given $z_{ij} = 1$, selected classical and QKD demands between q_i and q_j follow the bypass route.

IEEE Transactions on Quantum Engineering

IV. PROBLEM FORMULATION

This work aims to deploy the QCI at a minimum cost so that all QNs are connected with a minimum number of TRNs and the QKD requests are served by assigning the relay path with minimum energy consumption. In this work, we assume that servicing a QKD request with SKR demand r_k requires delivering the key rate where the observed QBER on the chosen path always stays within the operational range of the equipment. The objective is formally represented as:

$$P1: \underset{x,y,z}{\text{Minimize}} \left[\gamma_1 \mathcal{C}^{\text{CAP}} + \gamma_2 \mathcal{C}^{\text{OP}}\right] \tag{16}$$

subject to

$$\sum_{e_{ij} \in \mathcal{E}_i^T} x_{ij} \geq 1, \forall q_i \in \mathcal{V}^Q, \tag{17}$$

$$x_{ij} w_{ij} \leq W, \forall e_{ij} \in \mathcal{E}, \tag{18}$$

$$\sum_{f_k \in \mathcal{F}} y_{ij}^k r_k \leq x_{ij} r_{ij}, \forall e_{ij} \in \mathcal{E}, \tag{19}$$

$$\sum_{q_j \in \mathcal{V}^T} y_{ij}^k - \sum_{q_j \in \mathcal{V}^T} y_{ji}^k = \begin{cases} 1 & \text{if } q_i = q_k^{\text{src}}, \\ -1 & \text{if } q_i = q_k^{\text{dest}}, \\ 0 & \text{otherwise}, \end{cases} \forall f_k \in \mathcal{F}^Q, \tag{20}$$

$$y_{ij}^k + y_{ji}^k \leq x_{ij}, \forall e_{ij} \in \mathcal{E}, \forall f_k \in \mathcal{F}^Q, \tag{21}$$

$$\sum_{f_k \in \mathcal{F}^b} r_k \leq z_{ij} r_{ij}^*, \tag{22}$$

$$x_{ij}, y_{ij}^k, z_{ij} \in \{0,1\}, \forall e_{ij} \in \mathcal{E}, \forall f_k \in \mathcal{F}^Q, \tag{23}$$

where W is the link attenuation limit and r_{ij}^* is the SKR of the bypass route between q_i and q_j. The weight coefficients γ_1 and γ_2 define the weightage on the CAPEX and OPEX. $\mathcal{E}_i^T \subset \mathcal{E}^T$ denotes the set of links incident to q_i. Constraint (17) ensures that each QN is connected to G^T. Constraint (18) states that the attenuation of a link added to the minimum QCI should be within the attenuation limit of the quantum transceiver pair. Constraint (19) ensures that the aggregated key rate of the QKD requests relayed over a link should not exceed the SKR of the link. The flow conservation constraint for the QKD requests is Constraint (20). Constraint (21) states that a QKD request can be relayed through a link only if it is in G^T. Constraint (22) specifies that a bypass link between two nodes should be capable of accommodating all encrypted traffic between the nodes in terms of SKR. Constraint (23) mentions the binary decision variables.

V. TAQNET: THE PROPOSED SCHEME

The problem P1 is a BILP problem which is computationally expensive due to many constraints and binary decision variables, especially for large-scale QCI deployment. Therefore, to obtain a sub-optimal yet efficient solution, we decompose P1 into three sub-problems as follows:

$$SP1: \underset{x}{\text{Minimize}}\ \mathcal{C}^{(1)} = \left[\gamma_1 \mathcal{C}^{\text{CAP}} + \gamma_2 \mathcal{C}^{\text{OP}}\right] \tag{24}$$

subject to

(17), (18),

$$x_{ij} r_{ij} \geq \sum_{f_k \in \mathcal{F}} \bar{y}_{ij}^k r_k, \forall e_{ij} \in \mathcal{E}, \tag{25}$$

$$x_{ij} \geq \bar{y}_{ij}^k + \bar{y}_{ji}^k, \forall e_{ij} \in \mathcal{E}, \forall f_k \in \mathcal{F}^Q, \tag{26}$$

$$x_{ij} \in \{0,1\}, \forall e_{ij} \in \mathcal{E}. \tag{27}$$

$$SP2: \underset{y}{\text{Minimize}}\ \mathcal{C}^{(2)} = \left[\gamma_1 \mathcal{C}^{\text{CAP}} + \gamma_2 \mathcal{C}^{\text{OP}}\right] \tag{28}$$

subject to

(20),

$$\sum_{f_k \in \mathcal{F}} y_{ij}^k r_k \leq \bar{x}_{ij} r_{ij}, \forall e_{ij} \in \mathcal{E}, \tag{29}$$

$$y_{ij}^k + y_{ji}^k \leq \bar{x}_{ij}, \forall e_{ij} \in \mathcal{E}, \forall f_k \in \mathcal{F}^Q, \tag{30}$$

$$y_{ij}^k \in \{0,1\}, \forall e_{ij} \in \mathcal{E}, \forall f_k \in \mathcal{F}^Q. \tag{31}$$

$$SP3: \underset{z}{\text{Minimize}}\ \mathcal{C}^{(3)} = \left[\gamma_1 \mathcal{C}^{\text{CAP}} + \gamma_2 \mathcal{C}^{\text{OP}}\right] \tag{32}$$

subject to

(22),

$$z_{ij} \in \{0,1\}, \forall e_{ij} \in \mathcal{E}. \tag{33}$$

SP1 selects edges to include in the minimum QCI, while SP2 places QKD requests on the selected edges, and SP3 selects the bypass routes. Considering a scenario without any optical bypass and the coupling between the decision variables of SP1 and SP2, we solve SP1 and SP2 iteratively until convergence, as shown in Algorithm 1. The algorithm takes initial values of x and y, which are computed by generating MST using standard algorithms such as Kruskal's and Prim's and distributing the traffic randomly over the links in the MST. Based on the solutions SP1 and SP2, we propose a heuristic algorithm to reduce the QCI cost further by employing an optical bypass technique.

A. MINIMUM QCI DEPLOYMENT

We propose a heuristic solution for constructing the minimum-cost QCI G^T to reduce the complexity of large-scale deployments. To derive the minimum QCI, we model SP1 defined in (24) as the Steiner tree problem (STP) [28]. STP considers a connected undirected graph where each link has an associated cost. The STP involves discovering a tree with the lowest cost encompassing all the network terminal nodes. This tree may also include additional nodes from the network, known as Steiner nodes. For our problem, we consider the QNs as terminal nodes, TRNs as Steiner nodes, and the weight of a link e_{ij} is defined as $\mathcal{C}_{ij} = \mathcal{C}_{ij}^{\text{CAP}} + \mathcal{C}_{ij}^{\text{OP}}$, where $\mathcal{C}_{ij}^{\text{CAP}}$ and $\mathcal{C}_{ij}^{\text{OP}}$ are the CAPEX and OPEX for e_{ij}.

Algorithm 2 shows the steps of the minimum Steiner tree algorithm for QCI. The algorithm takes the graph of the integrated classical-quantum network G, the attenuation limit W, the initial y, and the weights γ_1 and γ_2 as inputs. The algorithm outputs the minimum-cost QCI G^T. To build the

Algorithm 1 Minimum QCI Formation and QKD Request Orchestration

INPUTS: Initial x and y, maximum number of iterations ($I_{\max}$), convergence tolerance (ϵ), $z = 0$
OUTPUT: Optimal x^* and y^*
PROCEDURE:
1: Set $I \leftarrow 0$ ▷ Iteration counter
2: Set converged $\leftarrow$ False ▷ Convergence flag
3: Set $x \leftarrow$ initial x, $y \leftarrow$ initial y
4: Set $U^* \leftarrow \mathrm{P1}(x, y, z)$ ▷ Optimal value
5: **while** $I \leq I_{\max}$ and not converged **do**
6: $x \leftarrow \mathrm{SP1}(y)$ using Algorithm 2
7: $y \leftarrow \mathrm{SP2}(x)$ using Algorithm 3
8: Compute $U \leftarrow \mathrm{P1}(x, y, z)$
9: **if** $|U^* - U| < \epsilon$ **then** ▷ Check convergence
10: Set converged $\leftarrow$ True
11: **end if**
12: $U^* \leftarrow U$
13: $I \leftarrow I + 1$
14: **end while**
15: **return** x^*, y^*

Algorithm 2 Steiner Tree Formation for Minimum QCI

INPUTS: G, W, y ,γ_1, γ_2
OUTPUT: G^T
PROCEDURE:
1: $\Psi \leftarrow \mathcal{V}^R$
2: $s \leftarrow$ Select the QN $q_i \in \mathcal{V}^Q$ that has the maximum number of QN-to-QN links
3: $\mathcal{V}^T \leftarrow \{s\}$
4: $\Psi \leftarrow \Psi \setminus \{s\}$
5: **while** $\Psi \neq \phi$ **do**
6: $MinWeight \leftarrow \infty$, $MinPath \leftarrow \phi$
7: **for each** $q_i \in \mathcal{V}^T$ **do**
8: Select the minimum weight path $Path_i$ with weight $\mathcal{C}_{ij}$ from q_i to a QN $q_j \in \Psi$ that satisfies constraints (18), (25), (26)
9: **if** $MinWeight \leq \mathcal{C}_{ij}$ **then**
10: Set $MinWeight \leftarrow \mathcal{C}_{ij}$, $MinPath \leftarrow Path_i$
11: **end if**
12: **end for**
13: Add the QNs and TRNs of $MinPath$ to $\mathcal{V}^T$ and add links of $MinPath$ to $\mathcal{E}^T$
14: Remove the QNs of $MinPath$ from Ψ
15: **end while**
16: **return** G^T

minimum-cost QCI, we select a starting QN. Line 2 selects the QN having the maximum number of neighbor QNs as the starting node for building G^T. This is to prioritize a central QN that is well-connected with other QNs. However, the selection of the starting QN can vary based on network management decisions. For instance, in topologies where certain nodes have high-demand characteristics or critical roles within the network, selecting these nodes as starting points may enhance overall network efficiency. Additionally, in networks with lower connectivity, choosing a peripheral node may allow for a more robust exploration of paths. Line 3 includes the starting QN to the minimum QCI G^T. The set of unvisited QNs is denoted by Ψ. Lines 5-15 form G^T and iterate until Ψ is empty. Algorithm 2 selects the minimum weight path from a QN in G^T to an unvisited QN in ψ. Line 13 adds the minimum cost path to G^T and Line 14 updates Ψ by removing the QNs added to the minimum QCI in the latest iteration.

As stated in Algorithm 2, the time complexity of forming a Steiner tree-based minimum QCI depends on the outer loop in Line 5, the inner loop in Line 7, and the selection of minimum cost path for each $q_j \in \Psi$ in Line 8. The computation of the minimum weight path with Dijkstra's algorithm implemented with Fibonacci heap and priority queue takes $\mathcal{O}(|\mathcal{E}|+|\mathcal{V}|\log|\mathcal{V}|)$ time [29]. Therefore, finding the minimum weight path from each node in $\mathcal{V}^T$ to each QN in Ψ takes $\mathcal{O}\big(|\mathcal{V}||\mathcal{V}^Q|(|\mathcal{E}|+|\mathcal{V}|\log|\mathcal{V}|)\big)$ time. Considering the outer loop, the worst-case time complexity of Algorithm 2 is $\mathcal{O}\big(|\mathcal{V}|^2|\mathcal{V}^Q|(|\mathcal{E}|+|\mathcal{V}|\log|\mathcal{V}|)\big) \approx \mathcal{O}\big(|\mathcal{V}|^2|\mathcal{V}^Q||\mathcal{E}|+|\mathcal{V}|^3|\mathcal{V}^Q|\log|\mathcal{V}|\big)$. However, in practice, the shortest path between each pair of nodes can be computed and stored in advance, and the time complexity of Algorithm 2 reduces to $\mathcal{O}(|\mathcal{V}|^2|\mathcal{V}^Q|)$.

B. QKD REQUEST ORCHESTRATION

The computation time for network planning to achieve minimum QCI deployment is not critical since it is conducted in advance. However, orchestrating QKD requests is an operational task requiring timely decisions. The formulated SP2 still incurs high costs concerning execution time as the network size and QKD demand grows. We design a GA-based meta-heuristic algorithm to handle the combinatorial nature of SP2 and provide near-optimal solutions within reasonable computational times. GA is particularly well-suited for this problem, as it efficiently navigates large solution spaces by emulating natural evolutionary processes. While alternative heuristic optimization methods, such as simulated annealing, may also be applicable, GA offers a robust balance between exploration and exploitation, making it highly effective for this combinatorial optimization task. GAs emulate natural evolution to explore solution spaces effectively, with individuals in the population representing potential solutions encoded by chromosomes. Recombination through selection and crossing operators generates new populations, aiming to produce promising solutions, while mutation operators introduce variation to prevent stagnation. GAs aim to balance exploiting known solutions and exploring new ones to find optimal solutions efficiently. Therefore, GA is an effective optimization technique spanning domains such as topological, combinatorial, and numerical problems [30]. The primary components of GA are as follows:

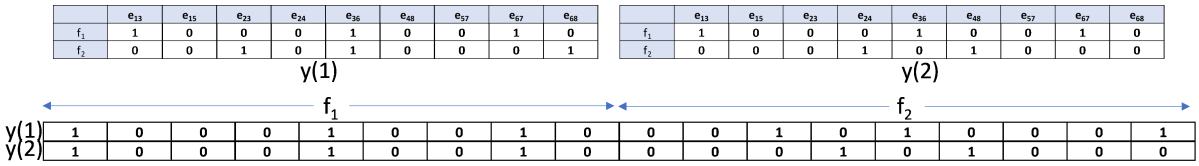

FIGURE 2: Example of chromosome formation

- **Chromosome**: In GA, each candidate solution represents a chromosome, an array of bits termed "gene". We formulate the chromosome ω based on the solution represented by the decision variable y which has the dimension $|\mathcal{V}| \times |\mathcal{V}| \times |\mathcal{F}^Q|$. For each QKD request f_k, we form a binary bit string where a bit referring to $e_{ij} \in \mathcal{E}$ is 1 if $y_{ij}^k = 1$. The bit strings of all requests are sequentially placed, forming a single bit string representing a candidate solution or chromosome. For example, Figure 2 shows the chromosome of 2 generations represented by solution variables $y(1)$ and $y(2)$ for QKD requests $f_1 \in \mathcal{F}^Q$ and $f_2 \in \mathcal{F}^Q$ based on the network depicted in Figure 1(a).
- **Population Initialization**: We generate the initial population by selecting random paths in G^T for each QKD request.
- **Fitness Function**: The fitness of an individual ω is estimated based on the optimization objective and respective constraints, and it is expressed as:
$$\text{fitness}(\omega) = C - (\mathcal{C}^{(2,\omega)} + \mathcal{C}^{(2,p)}), \quad (34)$$
where $C > 0$ is a large constant, $\mathcal{C}^{(2,\omega)}$ is the optimization objective for individual ω and $\mathcal{C}^{(2,p)}$ is the penalty term due to constraint (29). The penalty term is estimated as follows:
$$\mathcal{C}^{(2,p)} = \sum_{e=1}^{|\mathcal{E}|} \sum_{f_k \in \mathcal{F}^Q} \omega\big(e + (k-1)|\mathcal{E}|\big) r_k - r(e), \quad (35)$$
where $r(e) = r_{ij}$ if the e^{th} link is $e_{ij} \in \mathcal{E}$, $\omega(g)$ is the g^{th} gene of the individual ω.
- **Selection**: Two individuals are selected from the population as parents using deterministic tournament selection [30]. In this method, two individuals are randomly chosen, and the one with the highest fitness becomes the first parent. This process is repeated to select the second parent.
- **Crossover**: Two offspring are generated utilizing the two-point crossover technique. In this technique, we select the first crossover point CP_1 randomly from the set of gene locations $\{\omega\big(1+(k-1)|\mathcal{E}|\big) | 1 \le k \le |\mathcal{F}^Q|\}$. The second crossover point is $CP_2 = CP_1 + |\mathcal{E}| - 1$. This process ensures that a portion of the chromosome referring to a specific QKD request is selected for crossover. The first offspring is created by taking the genes from the beginning of the first parent to position $CP_1 - 1$, then taking the genes from CP_1 to CP_2 from the second parent, and finally taking the genes from position $CP_2 + 1$ to the end from the first parent. Similarly, the second offspring is created by taking the genes from the beginning of the second parent to position $CP_1 - 1$, then taking the genes from CP_1 to CP_2 from the first parent, and finally taking the genes from position CP_2+1 to the end from the second parent.
- **Mutation**: The mutation process introduces changes in the chromosomes. For this work, we consider that mutation entirely replaces a QKD request's path. Specifically, the genes associated with a randomly selected QKD request are replaced with a random E2E path. This strategy guarantees that the mutated QKD request is assigned to a complete E2E path rather than an incomplete one, thereby enhancing the reliability of the solution. Furthermore, the random selection of QKD requests facilitates broader exploration of the solution space, helping the algorithm to circumvent local minima and improve overall optimization performance.
- **Termination**: The execution of the GA algorithm terminates when the number of generations exceeds the upper bound GenMax or gap between the fitness of two consecutive solutions is less than the convergence tolerance ϵ_{GA}.

Algorithm 3 describes the steps of the proposed solution for finding the optimal placement of QKD requests. The algorithm takes the network parameters such as network graph G, set of QKD demands $\mathcal{F}^Q$, the minimum-cost QCI G^T, weight parameters γ_1, γ_2, and SKR matrix R with each element $r_{ij} \in R$ representing the SKR between q_i and q_j as inputs. Additional inputs to this algorithm are the GA parameters, such as the population size PS, maximum generations GenMax, and mutation probability P_m. We initialize the population of size PS by selecting random paths for each QKD request (Line 2). The algorithm then iterates over a loop for GenMax generations (Line 6). In each generation, parents are selected from the current population based on the fitness function as defined in (34) that evaluates the quality of paths (Line 7). These parents undergo crossover operations to produce two offspring (Line 8). The offspring are mutated to introduce variability (Line 9). The fitness of these offspring is then evaluated, and the best solution, denoted as ω^*, is updated if an improved solution is found (Line 10). This iterative process continues until the specified number of generations or the convergence is reached. Finally, as a solution of SP2, the algorithm outputs the optimal orchestration strategy y formed based on the best-found solution ω^*.

The time complexity of Algorithm 3 can be segregated into several components. The initialization phase, which

Algorithm 3 GA-Based QKD Request Orchestration

Input: $\mathcal{F}^Q$, G, G^T, γ_1, γ_2, SKR matrix R, population size PS, maximum generations GenMax, mutation probability P_m, convergence tolerance ϵ_{GA}
Output: y
Initialize population with randomly selected paths in G^T
Set $g \leftarrow 0$
converged $\leftarrow$ False
Set $\text{fit}_{\text{cur}} \leftarrow$ fitness based on y
while $g \leq \text{GenMax}$ and not converged **do**
    Select parents from population based on fitness function in (34)
    Perform crossover to generate two offspring
    Apply mutation to each offspring based on P_m
    Evaluate fitness of offspring and select the best solution ω^*; save best fitness fit_{best}
    $\text{fit}_{\text{cur}} \leftarrow \text{fit}_{\text{best}}$
    if $|\text{fit}_{\text{cur}} - \text{fit}_{\text{best}}| < \epsilon_{\text{GA}}$ **then**
        converged $\leftarrow$ True
    end if
    $g \leftarrow g + 1$
end while
Form y based on ω^*
return y

involves generating an initial population of PS paths, has a time complexity of $O(\text{PS})$. During each of the GenMax generations, several operations such as selection, crossover, mutation, and fitness evaluation are performed. The selection of parents based on fitness takes $O(\text{PS})$ time, assuming a linear selection mechanism. Further, the two crossover points are selected in $O(1)$ time and two offspring are generated in $O(|\mathcal{E}||\mathcal{F}^Q|)$ time as the length of a chromosome is $|\mathcal{E}||\mathcal{F}^Q|$. The mutation operation also takes $O(|\mathcal{E}||\mathcal{F}^Q|)$. Selecting the best offspring among the two for the current generation takes $O(1)$ time. Therefore, the time complexity of Algorithm 3 is $O\big(\text{PS} + \text{GenMax}(\text{PS} + |\mathcal{E}||\mathcal{F}^Q|)\big) \approx O\big(\text{GenMax}(\text{PS} + |\mathcal{E}||\mathcal{F}^Q|)\big)$, which can be managed by careful selection of the GA parameters PS and GenMax.

C. BYPASS ROUTE SELECTION

We design a greedy heuristic algorithm to identify potential bypass routes that reduces the overall cost as a solution to SP3. The steps of the proposed solution are shown in Algorithm 4. It takes classical demand D^C, QKD demand D^Q, the set of QKD requests $\mathcal{F}^Q$, network graph G, QKD request orchestration strategy y, and energy savings lower bound C^{lb} as inputs. The algorithm returns the bypass route selection strategy as output z. For every node pair (q_i, q_j), the existence of a potential bypass route is assessed. To determine the energy savings with optical bypass between q_i and q_j, we identify the set of QKD requests that has q_i and q_j on its route as specified by y which is generated by Algorithm 3. We select the requests in descending order

Algorithm 4 Greedy Bypass Route Selection

1: **Input:** D^C, D^Q, $\mathcal{F}^Q$, G, y, energy savings lower bound C^{lb}
2: **Output:** z
3: **for each** node pair q_i and $q_j \in \mathcal{E}$ **do**
4: Identify the set of potential QKD requests having q_i and q_j on their route defined by y
5: Select the QKD requests in descending order of key rate from the identified request set, provided that Constraint (22) is not violated
6: Using (14), estimate energy savings caused by assigning the classical demand between q_i and q_j and selected QKD requests to the bypass route
7: **end for**
8: Set $z_{ij} \leftarrow 1$ if the bypass route between q_i and q_j saves the maximum energy greater than C^{lb}
9: **return** z

of key rate from the identified request set provided that Constraint (22) is not violated. This approach ensures that the most impactful requests offering the most significant potential for OPEX reduction are considered first. Line 6 estimates energy savings caused by assigning the selected QKD requests and classical demands between q_i and q_j to a bypass route. As stated in Equation (16), the objective of this work includes the minimization of the OPEX, which consists of power consumption by both classical and quantum components, as given in Equation (14). Therefore, Algorithm 4 jointly considers energy savings for classical demand bypass and QKD bypass. A bypass route between q_i and q_j is selected if it saves the maximum energy greater than C^{lb}. Finally, the algorithm returns the bypass route selection strategy z. In this work, for simplicity, we assume that all classical demands and selected QKD demands having the bypass route end nodes on their route that satisfy Constraint (22) are considered for bypass. Accordingly, the set of QKD requests satisfying Constraint (22) constitutes $\mathcal{F}^b$. However, it is also possible for users to specify which classical and QKD requests should be eligible for bypass based on their requirements.

Algorithm 4 takes $O(|\mathcal{F}^Q| \log |\mathcal{F}^Q|)$ time to identify the potential QKD requests and estimate cost savings with selected requests in descending order of key rate (Lines 4-7). The loop in Line 3 iterates for $|\mathcal{E}|$ times. Therefore, the time complexity of Algorithm 4 is $O(|\mathcal{E}||\mathcal{F}^Q| \log |\mathcal{F}^Q|)$. We assume that all potential bypass routes are pre-computed and stored for efficient $O(1)$ lookup.

D. DEPLOYMENT STRATEGY FOR TAQNET

In practice, the network operator determines the appropriate timing for solving the subproblems SP1, SP2, and SP3. SP1, which focuses on selecting edges for the minimum QCI, should be addressed in advance, particularly during the initial stages of network setup or when significant changes

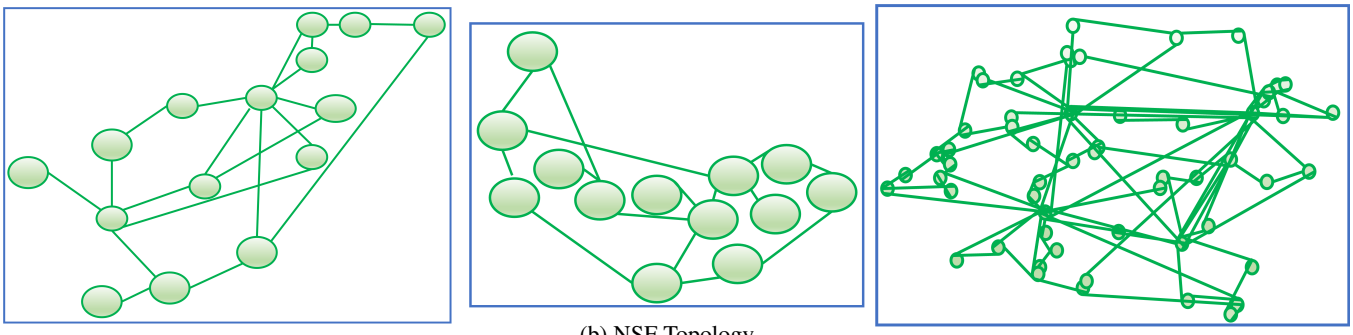

(a) Restena Topology (b) NSF Topology (c) DFN Topology

FIGURE 3: Network topologies used for simulation

in network topology or demand occur. By identifying the most cost-effective edges, operators can optimize the foundational structure of the quantum network. Following this, SP2, which orchestrates QKD requests, should be solved periodically or upon the arrival of new requests. This ensures that resource allocation reflects current network conditions and traffic demands, leading to optimal utilization of the established QCI. SP3, involving bypass route selection, can be addressed dynamically, especially during high-demand periods or when specific paths become congested or fail. This dynamic approach enhances network reliability.

The binary decision variables indicating edge selection for minimum QCI, QKD request orchestration, and bypass route selection are translated into actionable configurations for network hardware. For SP1, the decision variables (edges included in the QCI) inform the configuration of the underlying infrastructure to establish the minimum required connections for quantum communications. In SP2, the decision variables (which QKD requests are allocated to which paths) guide the routing configurations, managing how QKD traffic is directed across the established QCI. For SP3, selected bypass routes can be configured. These decision variables should be reviewed and updated regularly or in response to significant changes in network conditions, such as fluctuations in demand, topology adjustments, or failures.

Critical factors such as security and flexibility must also be prioritized for TAQNet deployment. Implementing robust security protocols to protect the QKD process is essential, ensuring that paths selected for QKD requests are secure and free from potential eavesdropping. Furthermore, the network should exhibit flexibility to accommodate dynamic adjustments in response to fluctuating demands, including the ability to rapidly adapt to new QKD requests and changes in network topology.

VI. PERFORMANCE EVALUATION

A. SIMULATION SETTINGS

We evaluate the performance of TAQNet through MATLAB simulations, available as a desktop application[1]. The classical traffic demand in Gbps between nodes pair is generated using uniform random distribution $\{10, 2X-10\}$ with traffic intensity $X \in \{20, 40, \ldots, 120\}$ [27]. For the simulation, we assume that QKD demand is proportional to the classical demand with $\zeta = 10^{-6}$ and set the number of QKD requests to 10 as a default value. We also consider a guard band of 200 GHz to mitigate the effects of SRS [18]. We consider three different topologies – Restena with 15 nodes [31], NSF with 13 nodes, and DFN with 58 nodes [32] as shown in Figure 3. We randomly divide the nodes into two sets for QNs and TRNs for each topology, respectively. Table 2 states simulation parameters and Table 3 shows the GA parameters. These parameters may require adjustments as the solution space scales, particularly with more complex network topologies. For instance, the mutation probability might need to be increased to introduce more diversity in the population, allowing the algorithm to explore a broader range of potential solutions and avoid local optima. Similarly, increasing the population size or the number of generations may improve convergence toward a better solution, but this comes at the cost of higher computational overhead. We show a 95% confidence interval for each simulation result.

[1]https://github.com/IloraMaity/TAQNet_App

B. BENCHMARK SCHEME

We compare TAQNet with the optimal solution generated using CVX [36]. In addition, we compare the proposed solution with another benchmark referred to as MST-Baseline, where the edges for the QCI are selected based on the standard MST, and the quantum traffic is randomly distributed over the links in the MST.

C. PERFORMANCE METRICS

- **TRNs in Minimum QCI**: This metric expresses the percentage of TRNs included in the minimum QCI compared to the TRNs in the entire network, i.e., $\frac{|\mathcal{V}^R \cap \mathcal{V}^T|}{|\mathcal{V}^R|} \times 100$.
- **CAPEX**: This metric quantifies the cost for deploying a minimally connected QCI as stated in (11). For an extensive evaluation of CAPEX, we assume that deploying new fibers is required to set up the QCI.

TABLE 2: Simulation parameters

Parameter	***Value***	***Parameter***	***Value***
Network topology	Restena [31], NSF, and DFN [32]	Number of signal pulses sent during an hour	3.24×10^{12} [33]
Number of QNs	10 (Restena), 9 (NSF), and 39 (DFN)	Number of QKD requests	$2 - 10$
Number of TRNs	5 (Restena), 4 (NSF), and 19 (DFN)	γ_1, γ_2	0.5
Number of QKD links	20 (Restena), 15 (NSF), and 87 (DFN)	Number of classical channels (N^C)	4
Cost of deploying a QN (c^Q)	20000 US$ [9]	Number of quantum channels (N^Q)	$1 - 4$
Cost of deploying a TRN (c^R)	15000 US$ [9]	Channel spacing (δ)	100 GHz [21]
Cost per kilometer of a channel on a fiber link (c^L)	5 US$ [9]	Guard band (B^{guard})	200 GHz [21]
Attenuation of a link per km (w)	$0.1 - 0.5$ dB	Transmission capacity of each channel (B)	50 Gbps [34]
Alignment of optical system (β)	0.033 [10]	Span distance between two neighboring EDFAs (S)	80 km [14]
Average photon flux (μ)	0.48 [10]	Power consumption per router port (E^r)	1000 W [35]
Detection efficiency ($\eta_i \eta_{\text{spd}}$)	0.045 [10]	Power consumption per transponder (E^t)	73 W [35]
Error correction inefficiency factor function ($f(QBER)$)	1.22 [10]	Power consumption per EDFA (E^e)	8 W [35]
Dark count probability (P_{dark})	0.85×10^{-6} [23]	Power consumption per QKD transceiver (E^{tr})	73 W
Maximum number of iterations ($I_{\max}$)	10	Convergence tolerance (ϵ)	0.1

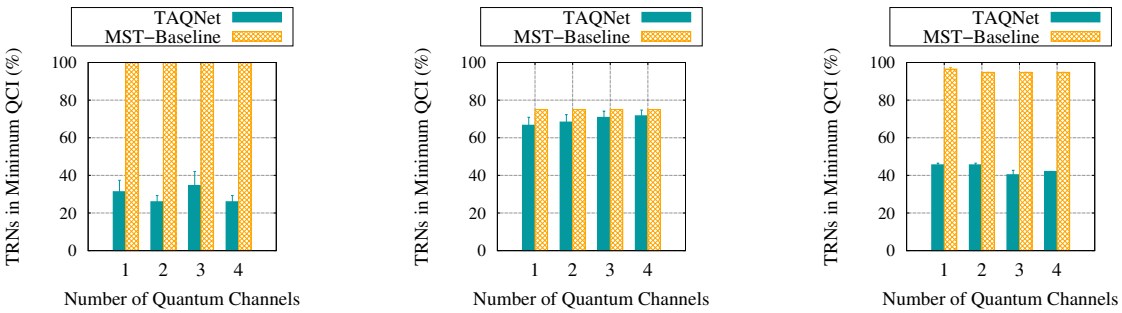

(a) Restena topology (b) NSF topology (c) DFN topology

FIGURE 4: TRNs in minimum QCI

TABLE 3: GA parameters

Parameter	***Value***
Population size (PS)	20
Number of generations (GenMax)	10
Mutation probability (P_m)	0.1
Convergence tolerance (ϵ_{GA})	0.1

- **Power Consumption by Quantum Components**: This metric estimates the power consumed due to placing quantum demands on the multiplexed links. It is estimated using (13).
- **Energy Efficiency**: This metric estimates the energy consumption in terms of kbit per Joule.

D. RESULT AND DISCUSSION

1) TRNs in Minimum QCI

Figure 4 shows that the number of TRNs in the minimum QCI is smaller for TAQNet than for MST-Baseline. A low TRN count reduces the CAPEX defined in (11). Algorithm 2 constructs the minimum QCI by prioritizing the links with low weight, formulated based on the CAPEX for the respec-

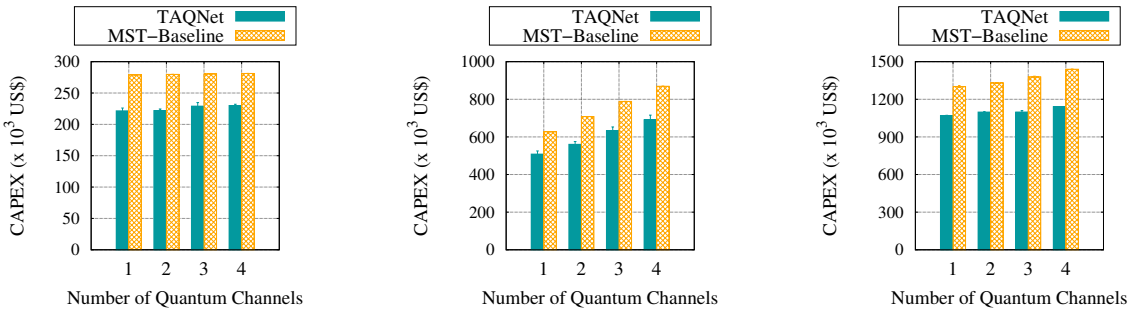

(a) Restena topology (b) NSF topology (c) DFN topology

FIGURE 5: CAPEX

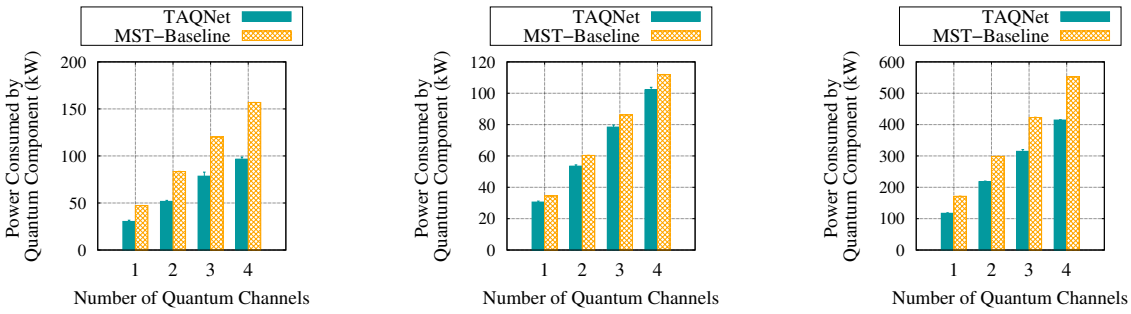

(a) Restena topology (b) NSF topology (c) DFN topology

FIGURE 6: Power consumption by quantum components

tive links. Therefore, the number of TRNs in the minimum QCI reduces. We also observe that TAQNet performs well for different quantum channels coexisting with classical channels. As formulated in (10), the quantum link deployment cost increases with the number of quantum channels. In this case, Algorithm 2 adds shorter paths connecting unvisited QNs to the minimum QCI, lowering the TRN count. In addition, from the simulation results, we observe that the TRN count in the minimum QCI solution by TAQNet depends on the dimension and connectivity of the topology. For example, although having a similar node count, the performance gap for NSF is lower than that for Restena as NSF is less well-connected than Restena, implying fewer alternatives for constructing the minimum QCI. Also, for large-scale topologies such as DFN, the percentage of TRNs utilized to construct the minimum QCI is smaller as the topology is well-connected.

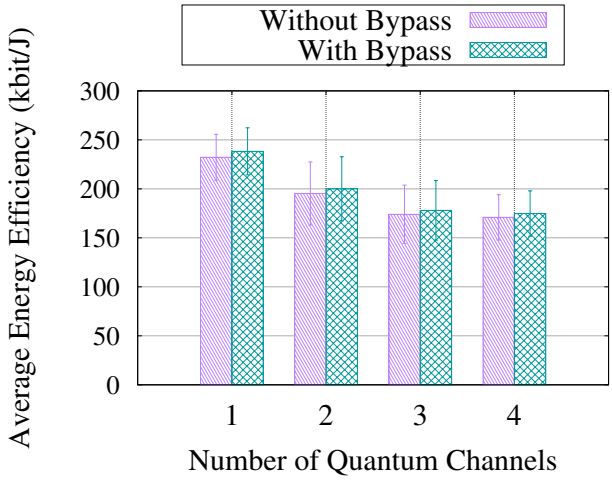

FIGURE 7: Energy efficiency for Restena topology

2) CAPEX

From Figure 5, we observe that TAQNet reduces CAPEX significantly compared to the benchmark for all three topologies. For example, the CAPEX of TAQNet for the Restena topology is 19.41% less than that of the MST-Baseline. This is because the Algorithm 2 starts with a maximally connected QN and continues to grow the minimum QCI by adding a minimum number of TRNs. Hence, the total fiber length is reduced, which minimizes the quantum link deployment cost and the CAPEX. The CAPEX increases with the number of quantum channels. This is because of the increase in the quantum link deployment cost formulated in (10). However, the simulation results demonstrate a steady performance gap for varying quantum channels. TAQNet balances the trade-off between the number of channels and CAPEX by selecting shorter paths while forming the minimum QCI. Also, we observe that the CAPEX increases with the topology dimension as more nodes and longer links are deployed. Less connected topology NSF has higher CAPEX than Restena due to the limited availability of shorter paths for the minimum QCI.

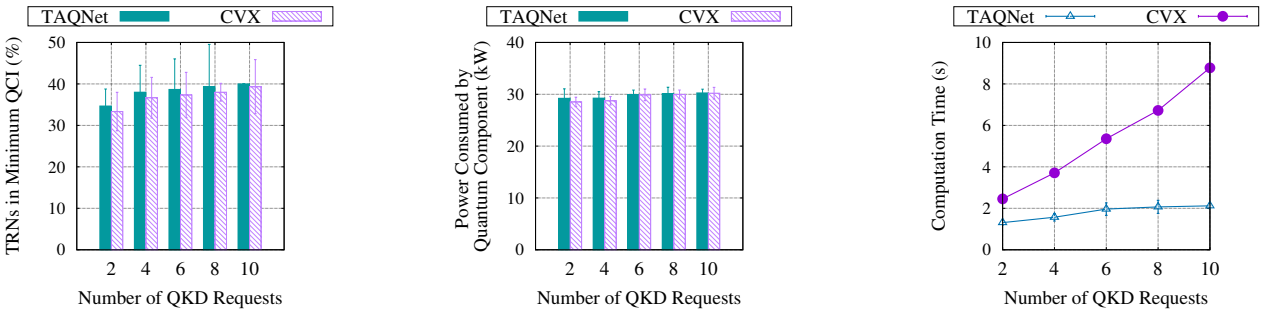

(a) TRNs in minimum QCI (b) Power consumed by quantum components (c) Computation time

FIGURE 8: Comparision with the optimal solution for Restena topology

3) Power Consumption by Quantum Components

As shown in Figure 6, TAQNet reduces power consumption by quantum components compared to the benchmark. In particular, the power consumption for TAQNet is 36.91% and 9.62% less than that of the benchmark for Restena and NSF topology, respectively. As defined in (13), the power consumption of quantum components mainly depends on the number of quantum channels and the QKD traffic distribution. TAQNet optimizes the QKD traffic distribution based on the fitness function in (34) that aims to reduce the OPEX. Therefore, as the number of quantum channels increases, the GA algorithm searches for more optimal QKD request orchestration to avoid excessive power consumption. In addition, we observe that the power consumption depends on the number of nodes in the topology. For Restena and NSF, which have fewer nodes, the power consumption is lower than that for DFN, which has a significantly higher number of nodes. This is because the power consumption of router ports at each node is the main contributor to the power consumption, as stated in (13). TAQNet balances the QKD traffic at each node to control this power usage.

4) Energy Efficiency

Optical bypass reduces the energy consumption at the router port by bypassing intermediate nodes. Figure 7 shows the average energy efficiency for Restena topology with and without E2E bypass routes. The simulation results show that optical bypass is more energy efficient compared to non-bypass. In particular, with optical bypass, TAQNet is 2.6% more energy efficient with a single quantum channel coexisting with classical channels. As outlined in Algorithm 4, the bypass route that maximizes energy savings is chosen for each node pair. Accordingly, the average energy efficiency signifies the average for selecting only a single bypass route considering all node pairs. The energy efficiency can be further improved by increasing the number of bypass routes, especially in larger or more complex topologies.

5) Comparison with Optimal Solution

We utilized CVX to compute the optimal solution for P1 under a non-bypass scenario with a different number of QKD requests. Figure 8 compares the CVX solution with the TAQNet solution for the Restena topology. From the simulation results, we observe that TAQNet achieves performance comparable to the CVX solution regarding the number of TRNs within the minimum QCI and the power consumption by quantum components. However, the computation time for the CVX solution increases exponentially with the number of QKD requests, rendering it impractical for large-scale or dynamic networks. Despite this limitation, in scenarios where the QCI is static, and the QKD request set is relatively fixed, the fully optimal CVX solution may offer advantages due to its ability to determine the global optimum. Thus, while TAQNet is designed to provide scalability and efficiency for high-traffic and large-scale networks, CVX remains a viable approach for smaller, static networks where optimality is prioritized over scalability.

6) Effect of SRS Noise

To evaluate the effect of SRS noise on QBER, we perform a set of simulations with no guard band separation between quantum and classical channels. For this simulation, we allocate N^Q quantum channels at shorter wavelengths starting with 1530 nm and N^C classical channels at longer wavelengths. However, the optimal quantum channel locations can be selected as proposed by Lin et al. [10]. We set the average launch power of classical channels to -20 dBm. The detection gate length is 2.5 ns, and the average signal photon number per time interval is 0.5. For co-propagating, the SRS coefficient slopes per channel per km for Stokes and anti-Stokes are set to 6.9×10^{-12} and 11.5×10^{-12}, respectively. For counter-propagating, the SRS coefficient slopes per channel per km for Stokes and anti-Stokes are set to 6.8×10^{-12} and 10.8×10^{-12}, respectively [10].

Figure 9 shows the effect of SRS noise for co- and counter-propagation cases for Restena topology in terms of the power consumed by quantum components. From the simulation results, we observe that the power consumption is higher for co-propagation case compared to that for counter-propagation case. This is because the SRS noise is higher for co-propagation which increases the QBER and the QKD request orchestration is less optimized as a result.

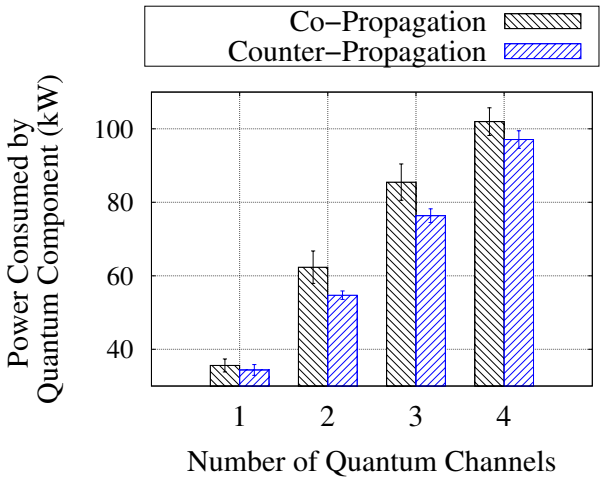

FIGURE 9: Effect of SRS noise for Restena topology

The simulation results show that TAQNet significantly improves the efficiency and cost-effectiveness of the QCI. It effectively manages the quantum-classical coexistence and maintains performance across various numbers of quantum channels and topologies. Optical bypass technology further enhances network sustainability with energy savings.

VII. CONCLUSION

In conclusion, this paper presents a traffic-aware minimum-cost quantum communication network planning approach, named TAQNet, for optimizing the deployment of QCIs by jointly considering TRN placement and QKD request orchestration while accommodating quantum-classical coexistence. Through our proposed Steiner tree-based methodology, we effectively deploy a minimally connected QCI, considering both CAPEX and OPEX. Our algorithm constructs a minimum Steiner tree for QCI deployment and offers a heuristic solution for orchestrating QKD requests across the minimum QCI to meet key rate demands. Additionally, we introduce a heuristic algorithm to identify feasible routes for optical bypassing, further reducing QCI costs. Evaluation of real-world network topologies demonstrates significant efficiency gains, with the proposed scheme reducing the power consumption by quantum components by 36.91% and CAPEX by 19.41% in the minimum QCI for the Restena topology compared to the MST-Baseline benchmark.

As a prospective extension, we envision leveraging satellite-based QKD links to reduce TRN numbers dynamically. Moreover, we aim to enhance the algorithm to accommodate preference for specific topologies (e.g., star) during the minimum QCI construction, improving flexibility and adaptability in QCI deployment strategies. Also, we plan to consider dynamic QKD requests and heterogeneous TRNs with varying resource capacity that influences network planning. Future work could also explore the integration of entanglement swapping to extend the QKD range and reduce TRN usage. Additionally, investigating the impact of different traffic patterns on QCI performance and developing strategies for adaptive reconfiguration of QCI under varying network conditions are essential areas for further research. Also, investigating the applicability of advanced QKD protocols such as E91 and MDI is another area of future research. Open questions remain on efficiently managing QCI resources in large-scale networks and balancing the trade-offs between cost, security, and performance in diverse deployment scenarios.

REFERENCES

[1] L. Le and T. N. Nguyen, "DQRA: Deep Quantum Routing Agent for Entanglement Routing in Quantum Networks," IEEE Transactions on Quantum Engineering, vol. 3, pp. 1–12, 2022.
[2] S. Kisseleff and S. Chatzinotas, "Trusted Reconfigurable Intelligent Surface for Multi-User Quantum Key Distribution," IEEE Communications Letters, pp. 1–1, 2023.
[3] W. Kong, Y. Sun, Y. Gao, and Y.-F. Ji, "Coexistence of quantum key distribution and optical communication with amplifiers over multicore fiber," Nanophotonics, vol. 12, pp. 1979 – 1994, 2023.
[4] K. A. Patel, J. F. Dynes, I. Choi, A. W. Sharpe, A. R. Dixon, Z. L. Yuan, R. V. Penty, and A. J. Shields, "Coexistence of High-Bit-Rate Quantum Key Distribution and Data on Optical Fiber," Phys. Rev. X, vol. 2, p. 041010, Nov 2012.
[5] Y. Cao, Y. Zhao, Q. Wang, J. Zhang, S. X. Ng, and L. Hanzo, "The Evolution of Quantum Key Distribution Networks: On the Road to the Qinternet," IEEE Communications Surveys & Tutorials, vol. 24, no. 2, pp. 839–894, 2022.
[6] S. K. Patri, M. Wenning, S. H. Gonde, A. Autenrieth, J.-P. Elbers, and C. Mas-Machuca, "Trusted Node Deployment Strategies for Long-Haul Quantum Key Distribution Networks," in International Conference on Optical Network Design and Modeling (ONDM), 2023, pp. 1–6.
[7] N. K. Kundu, M. R. McKay, A. Conti, R. K. Mallik, and M. Z. Win, "MIMO Terahertz Quantum Key Distribution Under Restricted Eavesdropping," IEEE Transactions on Quantum Engineering, vol. 4, pp. 1–15, 2023.
[8] Q. Zhang, O. Ayoub, A. Gatto, J. Wu, X. Lin, F. Musumeci, G. Verticale, and M. Tornatore, "Joint Routing, Channel, and Key-Rate Assignment for Resource-Efficient QKD Networking," in IEEE Global Communications Conference, 2022, pp. 3676–3681.
[9] Y. Cao, Y. Zhao, J. Wang, X. Yu, Z. Ma, and J. Zhang, "Cost-efficient quantum key distribution (QKD) over WDM networks," Journal of Optical Communications and Networking, vol. 11, no. 6, pp. 285–298, 2019.
[10] R. Lin and J. Chen, "Modeling and Minimizing Spontaneous Raman Scattering for QKD Secured DWDM Networks," IEEE Communications Letters, vol. 25, no. 12, pp. 3918–3921, 2021.
[11] C. H. Bennett and G. Brassard, "Quantum cryptography: Public key distribution and coin tossing," Theoretical Computer Science, vol. 560, pp. 7–11, 2014.
[12] M. Sabani, I. Savvas, D. Poulakis, and G. Makris, "Quantum Key Distribution: Basic Protocols and Threats," in Pan-Hellenic Conference on Informatics, ser. PCI '22. New York, NY, USA: Association for Computing Machinery, 2023, p. 383–388. [Online]. Available: https://doi.org/10.1145/3575879.3576022
[13] H.-K. Lo, M. Curty, and B. Qi, "Measurement-Device-Independent Quantum Key Distribution," Phys. Rev. Lett., vol. 108, p. 130503, Mar 2012. [Online]. Available: https://link.aps.org/doi/10.1103/PhysRevLett.108.130503
[14] G. A. Beletsioti, G. I. Papadimitriou, and P. Nicopolitidis, "Energy-Aware Algorithms for IP Over WDM Optical Networks," Journal of Lightwave Technology, vol. 34, no. 11, pp. 2856–2866, 2016.
[15] I. Maity and S. Chatzinotas, "Cost-Efficient Network Planning for Quantum Communication Infrastructure," IEEE Globecom Workshops, 2023.
[16] M. Gunkel, F. Wissel, and A. Poppe, "Designing a Quantum Key Distribution Network - Methodology and Challenges," in Photonic Networks; ITG-Symposium, 2019, pp. 1–3.
[17] J.-Q. Geng, G.-J. Fan-Yuan, S. Wang, Q.-F. Zhang, Y.-Y. Hu, W. Chen, Z.-Q. Yin, D.-Y. He, G.-C. Guo, and Z.-F. Han, "Coexistence of quantum key distribution and optical transport network based on standard single-mode fiber at high launch power," Opt. Lett., vol. 46, no. 11, pp. 2573–2576, Jun 2021.

[18] N. A. Peters, P. Toliver, T. E. Chapuran, R. J. Runser, S. R. McNown, C. G. Peterson, D. Rosenberg, N. Dallmann, R. J. Hughes, K. P. McCabe, J. E. Nordholt, and K. T. Tyagi, "Dense wavelength multiplexing of 1550 nm QKD with strong classical channels in reconfigurable networking environments," New Journal of Physics, vol. 11, 2009.

[19] T. Shen, X. Wang, Z. Chen, H. Tian, S. Yu, and H. Guo, "Experimental Demonstration of LLO Continuous-Variable Quantum Key Distribution With Polarization Loss Compensation," IEEE Photonics Journal, vol. 15, no. 2, pp. 1–9, 2023.

[20] P. G. Evans, M. Alshowkan, D. Earl, D. D. Mulkey, R. Newell, G. Peterson, C. Safi, J. L. Tripp, and N. A. Peters, "Trusted Node QKD at an Electrical Utility," IEEE Access, vol. 9, pp. 105 220–105 229, 2021.

[21] Y. Cao, Y. Zhao, X. Yu, and Y. Wu, "Resource assignment strategy in optical networks integrated with quantum key distribution," Journal of Optical Communications and Networking, vol. 9, no. 11, pp. 995–1004, 2017.

[22] S. Guerrini, M. Chiani, and A. Conti, "Secure Key Throughput of Intermittent Trusted-Relay QKD Protocols," in IEEE Globecom Workshops (GC Wkshps), 2018, pp. 1–5.

[23] T. Ferreira da Silva, G. B. Xavier, G. P. Temporão, and J. P. von der Weid, "Impact of Raman Scattered Noise from Multiple Telecom Channels on Fiber-Optic Quantum Key Distribution Systems," Journal of Lightwave Technology, vol. 32, no. 13, pp. 2332–2339, 2014.

[24] X. Ma, B. Qi, Y. Zhao, and H.-K. Lo, "Practical decoy state for quantum key distribution," Phys. Rev. A, vol. 72, p. 012326, Jul 2005. [Online]. Available: https://link.aps.org/doi/10.1103/PhysRevA.72.012326

[25] H.-K. Lo, X. Ma, and K. Chen, "Decoy State Quantum Key Distribution," Phys. Rev. Lett., vol. 94, p. 230504, Jun 2005. [Online]. Available: https://link.aps.org/doi/10.1103/PhysRevLett.94.230504

[26] M. Pistoia, O. Amer, M. R. Behera, J. A. Dolphin, J. F. Dynes, B. John, P. A. Haigh, Y. Kawakura, D. H. Kramer, J. Lyon, N. Moazzami, T. D. Movva, A. Polychroniadou, S. Shetty, G. Sysak, F. Toudeh-Fallah, S. Upadhyay, R. I. Woodward, and A. J. Shields, "Paving the way toward 800 Gbps quantum-secured optical channel deployment in mission-critical environments," Quantum Science and Technology, vol. 8, no. 3, p. 035015, May 2023. [Online]. Available: http://dx.doi.org/10.1088/2058-9565/acd1a8

[27] Y. Lui, G. Shen, and W. Shao, "Design for energy-efficient IP over WDM networks with joint lightpath bypass and router-card sleeping strategies," Journal of Optical Communications and Networking, vol. 5, no. 11, pp. 1122–1138, 2013.

[28] L. Martins, D. Santos, T. Gomes, and R. Girão-Silva, "Determining the Minimum Cost Steiner Tree for Delay Constrained Problems," IEEE Access, vol. 9, pp. 144 927–144 939, 2021.

[29] J. Gorst, "Time & Space Complexity of Dijkstra's Algorithm," 2023, Accessed: Jul 2023. [Online]. Available: https://iq.opengenus.org/time-and-space-complexity-of-dijkstra-algorithm/

[30] P. P. Cespedes-Sanchez, B. Maluff, D. P. Pinto-Roa, and H. Legal-Ayala, "Hybrid Incremental Deployment of HSDN Devices," IEEE Transactions on Network and Service Management, vol. 19, no. 2, pp. 1662–1678, 2022.

[31] Restena Foundation, "RESTENA Network," Accessed: Jul 2023. [Online]. Available: https://www.restena.lu/en/network

[32] S. Knight, H. Nguyen, N. Falkner, R. Bowden, and M. Roughan, "The Internet Topology Zoo," IEEE Journal on Selected Areas in Communications, vol. 29, no. 9, pp. 1765 –1775, october 2011.

[33] Y. Liu, W.-J. Zhang, C. Jiang, J.-P. Chen, D. Ma, C. Zhang, W.-X. Pan, H. Dong, J.-M. Xiong, C.-J. Zhang, H. Li, R.-C. Wang, C.-Y. Lu, J. Wu, T.-Y. Chen, L. You, X.-B. Wang, Q. Zhang, and J.-W. Pan, "1002 km twin-field quantum key distribution with finite-key analysis," Quantum Frontiers, vol. 2, no. 1, p. 16, November 24 2023. [Online]. Available: https://doi.org/10.1007/s44214-023-00039-9

[34] M. Mlejnek, N. A. Kaliteevskiy, and D. A. Nolan, "Reducing spontaneous Raman scattering noise in high quantum bit rate QKD systems over optical fiber," 2017.

[35] G. Shen and R. S. Tucker, "Energy-Minimized Design for IP Over WDM Networks," Journal of Optical Communications and Networking, vol. 1, no. 1, pp. 176–186, 2009.

[36] M. Grant and S. Boyd, "CVX: Matlab software for disciplined convex programming, version 2.1," https://cvxr.com/cvx, Mar. 2014.